contributions and all members of the laboratory for fruitful discussions. Plasmids used to generate recombinant influenza viruses are subject to a material transfer agreement. We thank members of the French Memo-Flu-ARDS study group (PIs: B. Autran, Inserm U945, and C.-E. Luyt, Service de réanimation médicale, Hôpital Pitié-Salpêtrière, Paris) for recruiting adult severe flu patients. Supported by National Center for Research Resources and National Center for Advancing Translational Sciences grant 8UL1TR000043; NIH grants 5R01NS072381 (J.-L.C. and L.D.N.), 5R01AI100887 (L.D.N.), and 1U19AI109945 (C.F.B.); the Rockefeller University, the St. Giles Foundation, the French National Research Agency under the "Investments for the Future" program grant ANR-10-IAHU-01, the Laboratoire d'Excellence Integrative Biology of Emerging Infectious Diseases (ANR-10-LABX-62-IBEID), INSERM, Paris Descartes University, and ERC grant 2010-StG-261299 (F.G.); and Center for Research on Influenza Pathogenesis and the NIAID-funded Center of Excellence for Influenza Research and Surveillance contract HHSN272201400008C (A.G.-S.). The data presented in this manuscript are tabulated in the main paper and in the supplementary materials. Raw data for the microarray analyses performed in this study are available from the public repository of GEO DataSets (accession no. GSE66486). The raw sequence data are available on the Sequence Read Archive (SRA) database: Bioproject SRP055919.

SUPPLEMENTARY MATERIALS

www.sciencemag.org/content/348/6233/448/suppl/DC1
Case Report
Materials and Methods
Supplementary Text
Figs. S1 to S9
Tables S1 to S7
References (*35*–*50*)

24 October 2014; accepted 12 March 2015
Published online 26 March 2015;
10.1126/science.aaa1578

NEUROBIOLOGY

SARM1 activation triggers axon degeneration locally via NAD$^+$ destruction

Josiah Gerdts,[1] E.J. Brace,[2] Yo Sasaki,[1] Aaron DiAntonio,[2,3] Jeffrey Milbrandt*[1,3]

Axon degeneration is an intrinsic self-destruction program that underlies axon loss during injury and disease. Sterile alpha and TIR motif–containing 1 (SARM1) protein is an essential mediator of axon degeneration. We report that SARM1 initiates a local destruction program involving rapid breakdown of nicotinamide adenine dinucleotide (NAD$^+$) after injury. We used an engineered protease-sensitized SARM1 to demonstrate that SARM1 activity is required after axon injury to induce axon degeneration. Dimerization of the Toll–interleukin receptor (TIR) domain of SARM1 alone was sufficient to induce locally mediated axon degeneration. Formation of the SARM1 TIR dimer triggered rapid breakdown of NAD$^+$, whereas SARM1-induced axon destruction could be counteracted by increased NAD$^+$ synthesis. SARM1-induced depletion of NAD$^+$ may explain the potent axon protection in Wallerian degeneration slow (Wld^S) mutant mice.

Cells undergo regulated self-destruction during development and in response to stresses (*1*). Axons, the longest cellular structures in the body, have a locally mediated self-destruction program that removes damaged axons but also promotes axon loss in the setting of neurological disorders (*2*). Axon degeneration is antagonized by the Wallerian degeneration slow (Wld^S) chimeric protein (*3*). The active moiety of Wld^S is the enzyme nicotinamide mononucleotide adenyltransferase 1 (Nmnat1), which synthesizes the essential cofactor nicotinamide adenine dinucleotide (NAD$^+$) (*4*), but the function of Nmnat1 and NAD$^+$ in axon protection remains unclear (*2*). The protein SARM1 (sterile alpha and TIR motif–containing 1; TIR, Toll–interleukin receptor) is an essential mediator of axon degeneration (*5*, *6*). SARM1 is a negative regulator of Toll-like receptor–activated transcriptional programs (*7*), but its mechanism for axon degeneration is unknown.

To investigate whether SARM1 functions before or after injury, we engineered a system to inactivate SARM1 with pharmacologic control. Protease-sensitized SARM1 (SARM^{ps}) contains a tobacco etch virus (TEV) protease consensus sequence between the sterile alpha motif (SAM) and TIR domains, which are both essential for SARM1 function (*6*). SARM^{ps} is thus cleaved and inactivated by TEV protease. SARM^{ps} was fused to the rapamycin-binding domain Frb and the N-terminal portion of split TEV protease (Ntev) (*8*) and coexpressed with C-terminal split TEV fused to FK*866* binding protein (Fkbp-Ctev), allowing rapamycin-induced cleavage (Fig. 1A and fig. S1). In dorsal root ganglion (DRG) neurons, cleavage of SARM^{ps} was mostly complete within 60 min of rapamycin treatment (Fig. 1B and fig. S2A). SARM^{ps} functionality was verified by expression of SARM^{ps} in isolated Sarm1$^{-/-}$ DRG neurons. When Sarm1$^{-/-}$ axons were severed (diagrammed in Fig. 1C), they remained intact after 24 hours, whereas axons of neurons expressing SARM^{ps} showed degeneration measured by axon morphometry (Fig. 1D), similar to wild-type axons. SARM^{ps} function was lost upon cleavage triggered by rapamycin in the presence of Fkbp-Ctev (Fig. 1, D and E) or by expression of full-length TEV (fig. S2B). Cleavage of SARM^{ps} initiated 12 hours before or up to 2 hours after axon transection fully suppressed axon degeneration measured 24 hours after axotomy. Because cleavage of SARM^{ps} after axons were disconnected from cell bodies resulted in protection, SARM1 must function after injury to promote degeneration.

SARM1 has no predicted enzymatic function but contains a TIR domain, which is the effector domain of Toll-like receptors (TLRs). Activation of TLRs results in dimerization of TIR domains that transmit a signal to cytosolic effector proteins (*9*). We tested whether multimerization of the TIR domain of SARM1 (sTIR) might induce axon degeneration. A minimal region of human SARM1 comprising sTIR and the adjacent multimerization (SAM) domains, but lacking the autoinhibitory N terminus (SAM-TIR), is constitutively active and promotes cell and axon destruction in cultured DRG neurons (*6*). Expression of this activated form of SARM1 in vivo in *Drosophila* motor (Fig. 2A) or sensory neurons (fig. S3) also caused cell and axon destruction. This degeneration was not observed in *Drosophila* expressing SAM-TIR harboring a disruptive sTIR mutation.

To evaluate the sufficiency of sTIR dimerization in axon destruction, we engineered a pharmacologically controlled dimerizable sTIR by fusing it to the rapamycin-binding domains Frb and Fkbp (Fig. 2B) (*10*). We expressed Frb-sTIR and Fkbp-sTIR in DRG neurons and found that sTIR dimerization by rapamycin induced axon fragmentation within 12 hours (Fig. 2C) and neuronal cell death within 24 hours (Fig. 2D). sTIR-induced toxicity did not require the inhibition of mammalian target of rapamycin (mTOR), because the rapamycin analog AP20187, which does not target mTOR, also stimulated axon degeneration in cells expressing the homodimerizable Fkbp^{F36V}-sTIR (*10*). SARM1 activation is thus sufficient to elicit axonal and neuronal destruction. Cell and axon degeneration were not induced upon dimerization of the TIR domains of TLR4 or the adaptor MYD88 (Fig. 2E).

We tested whether SARM1 promotes axon degeneration through a local mechanism. sTIR-induced degeneration does not require a physical connection between the axon and soma: Sarm1$^{-/-}$ axons persisted after severing; however, sTIR dimerization by AP20187 caused fragmentation of these severed segments within 12 hours (Fig. 2F). Dimerization of sTIR locally within axons also led to selective axon destruction. We grew DRG neurons in adjacent fluid compartments: one containing the cell bodies and proximal axons and the other containing only distal axons (Fig. 2G). Application of AP20187 to both compartments led to destruction of proximal and distal axons, whereas selective application to the distal

[1]Department of Genetics, Washington University Medical School, Saint Louis, MO, USA. [2]Department of Developmental Biology, Washington University Medical School, Saint Louis, MO, USA. [3]Hope Center for Neurological Disorders, Saint Louis, MO, USA.
*Corresponding author. E-mail: jmilbrandt@wustl.edu

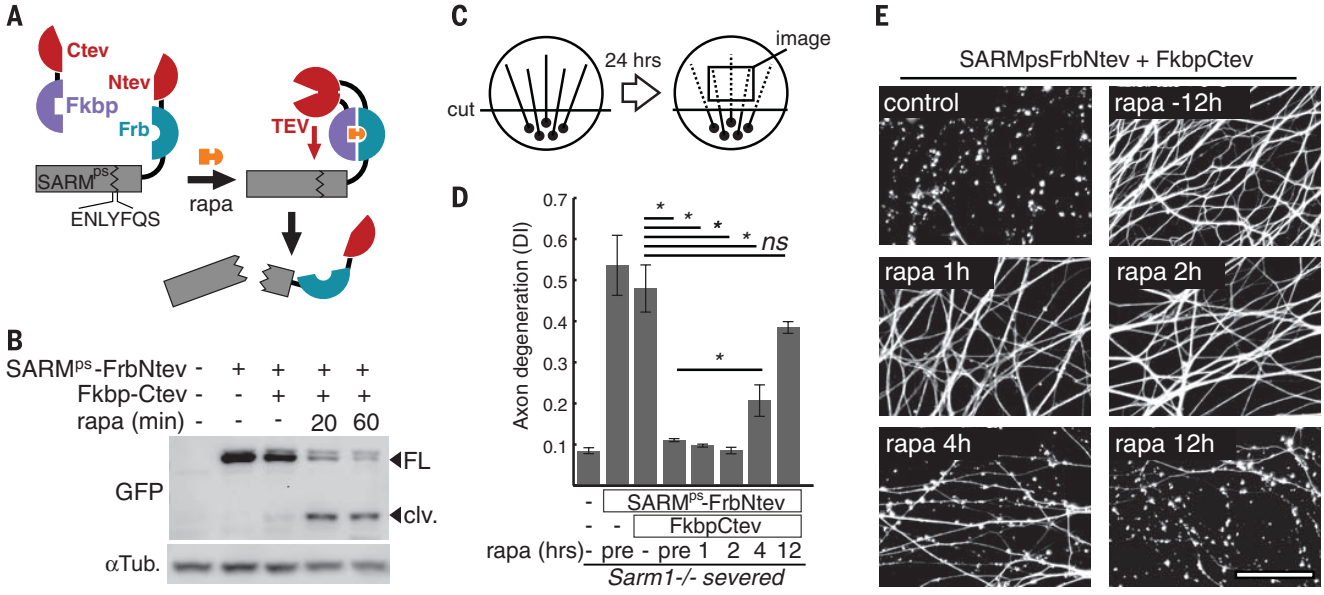

Fig. 1. SARM1 functions after axon injury to promote destruction. (**A**) Schematic showing how expression of SARM^{ps}-Frb-Ntev with Fkbp-Ctev allows rapamycin-induced complementation of split TEV and concomitant SARM^{ps} cleavage. (**B**) Gel electrophoresis with anti-GFP immunoblot showing SARM^{ps} cleavage in DRG neurons induced by 100 nM rapamycin (rapa); FL, full length SARM^{ps}-Frb-Ntev-Cerulean; clv, cleaved form. α-Tubulin (αTub) was a loading control. (C) Diagram of in vitro injury model: Isolated DRG neurons were severed, and axon degeneration was quantified from axon images after 24 hours. (**D**) Requirement for SARM1 activity after axotomy to induce axon degeneration. Axon degeneration is reported as the degeneration index (DI), a morphometric ratio of fragmented axon area to total axon area (*13*). Sarm1$^{-/-}$ DRG neurons treated with expression lentiviruses (control, SARMps-FrbNtev, and Fkbp-Ctev) were severed and treated with 100 nM rapamycin at various times (pre = 12 hours pre-injury). (**E**) Micrographs show representative α-tubulin–stained axons corresponding to select treatment groups in (D). Scale bar, 50 μm. Error bars, SEM; *P < 0.01; one-way analysis of variance (ANOVA) with Tukey's post-hoc test.

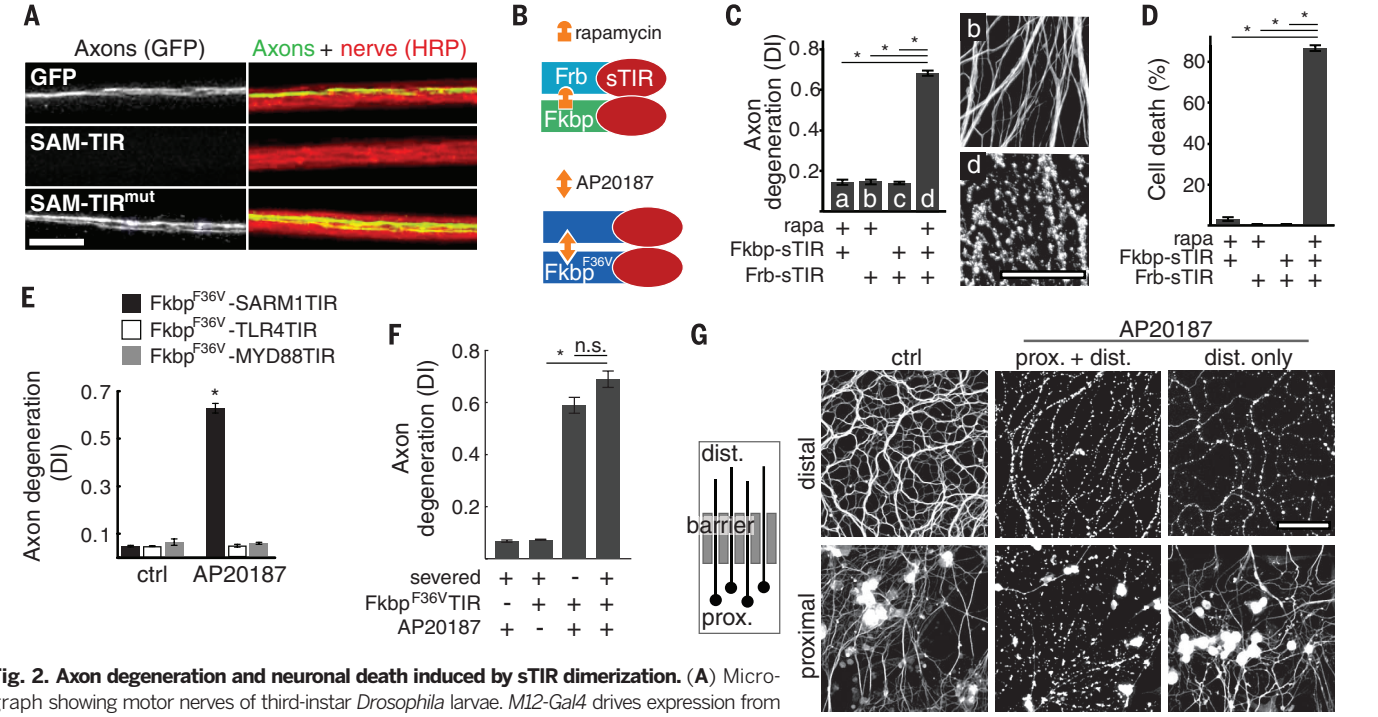

Fig. 2. Axon degeneration and neuronal death induced by sTIR dimerization. (**A**) Micrograph showing motor nerves of third-instar *Drosophila* larvae. *M12-Gal4* drives expression from mCD8-GFP (green) alone or with either UAS-SAM-TIR or UAS-SAM-TIR^{mut} in single motor axons in each nerve (red, HRP). UAS-SAM-TIR expression caused axon loss in 49 out of 49 (49/49) nerves as shown, whereas SAM-TIR with a disruptive TIR mutation led to degeneration in 0/70 nerves ($\chi 2 = 119$; $P < 0.001$); scale bar = 10 μm. (**B**) Schematic showing sTIR dimerization by rapamycin or AP20187. (**C**) Effect of sTIR, dimerized sTIR, and rapamycin on axon degeneration. α-Tubulin stained axons correspond to bars b and d. (**D**) Effect of sTIR dimerization on neuronal viability quantified by ethidium homodimer exclusion after 24 hours. (**E**) Effects of dimerization of sTIR or TIR domains of MYD88 or TLR4 on axon degeneration. (**F**) Effects of sTIR dimerization on degeneration of Sarm1$^{-/-}$ axons physically disconnected from cell bodies. (**G**) (Left) Diagram of axons growing through a diffusion barrier into an isolated fluid compartment. (Right) Micrographs of isolated distal axon segments after application of AP20187 globally or selectively to distal axons. Scale bar, 50 μm. Error bars, SEM; *P < 0.01; one-way ANOVA with Tukey's post-hoc test.

chamber elicited selective distal axon degeneration after 24 hours (Fig. 2G).

SARM1 TIR dimerization elicited rapid pathophysiologic changes: Axon degeneration and neuronal death were evident within 1.5 and 6 hours, respectively (fig. S4, A and B), and neuronal mitochondrial membrane potential dissipated and calcium accumulated with similar kinetics (fig. S4, C to E). These measurements indicate early energetic failure. We thus focused on biochemical events leading from SARM1 activation to axonal demise. Axon degeneration is antagonized by the NAD^+ synthetic enzyme Nmnat1, which, like SARM1, functions locally within axons (*11*). Injured axons exhibit declining levels of NAD^+ before morphologic changes (*12*), but it is unknown whether this is a cause or consequence of axon destruction. Although Wld^S/Nmnat1 does not increase the steady-state abundance of NAD^+ (*13*), in the setting of acute NAD^+ depletion it might maintain sufficient levels of NAD^+ for viability (diagrammed in Fig. 3A). We thus tested whether SARM1 activation leads to depletion of NAD^+.

To test whether endogenous SARM1 is necessary for axonal loss of NAD^+ after axotomy, we isolated axons from cultured wild-type and $Sarm1^{-/-}$ DRG neurons 3 and 4 hours after injury, a time when they remain morphologically intact, and measured the abundance of NAD^+ using high-performance liquid chromatography (HPLC). The abundance of NAD^+ decreased after injury in wild-type axons but remained stable in $Sarm1^{-/-}$ axons (Fig. 3B). Loss of adenosine triphosphate (ATP), an expected consequence of NAD^+ depletion, was also SARM1-dependent (fig. S5A). To determine whether SARM1 is also necessary for axotomy-induced loss of NAD^+ in vivo, we compared concentrations of NAD^+ in distal sciatic nerve segments from adult wild-type and $Sarm1^{-/-}$ mice. At 30 hours after injury, amounts of NAD^+ were decreased in wild-type nerves but remained stable in $Sarm1^{-/-}$ nerves (Fig. 3C). At this time, injured nerves remained morphologically intact (fig. S5C), and amounts of ATP were stable (fig. S5B).

We tested whether SARM1 activation was sufficient to elicit loss of NAD^+ by measuring neuronal NAD^+ after sTIR dimerization. sTIR dimerization by the addition of AP20187 caused rapid loss of NAD^+; within 15 min, the abundance of NAD^+ was reduced by 66%, and by 90 min, 90% of the NAD^+ was lost (Fig. 3D). The abundance of ATP also declined after sTIR dimerization, but its depletion was slower than that of NAD^+.

Together these data implicate NAD^+ loss as a critical step in SARM1-mediated axon destruction. We therefore examined whether increased NAD^+ synthesis could counteract the destruction program activated by sTIR dimerization. In DRG neurons, both axon degeneration and cell death initiated by sTIR dimerization were completely blocked by the expression of Nmnat1 and nicotinamide phosphoribosyltransferase (Nampt), which together synthesize NAD^+ (Fig. 3A). Protection appeared to require NAD^+ synthesis, because concurrent treatment with the Nampt inhibitor FK866 blocked the protection afforded by these enzymes (Fig. 3, E and F). Similarly, sTIR-induced axon degeneration and cell death were blocked by supplementation with the cell-permeant NAD^+ precursor nicotinamide riboside (NR) (Fig. 3, G and H) (*14*). *Drosophila* larvae expressing the dimerizable $Fkbp^{F36V}$-sTIR in motor neurons that were fed AP20187 showed extensive axon degeneration that was blocked by coexpression of cytosolic Nmnat1 (Fig. 3I).

To extend our analysis of biochemical events after SARM1 activation, we created a heterologous human embryonic kidney (HEK293T) cell line (HTir) that stably expresses Frb-sTIR and Fkbp-sTIR. After 12 hours of sTIR dimerization in HTir cells, toxicity was evident, as indicated by the loss of ATP (fig. S6A) and altered morphology (fig. S6B). Both effects were blocked by NR supplementation. Inhibition of NAD^+ synthesis with FK866 increased the loss of ATP, whereas FK866 was not toxic in the absence of sTIR dimerization (fig. S6, A and B).

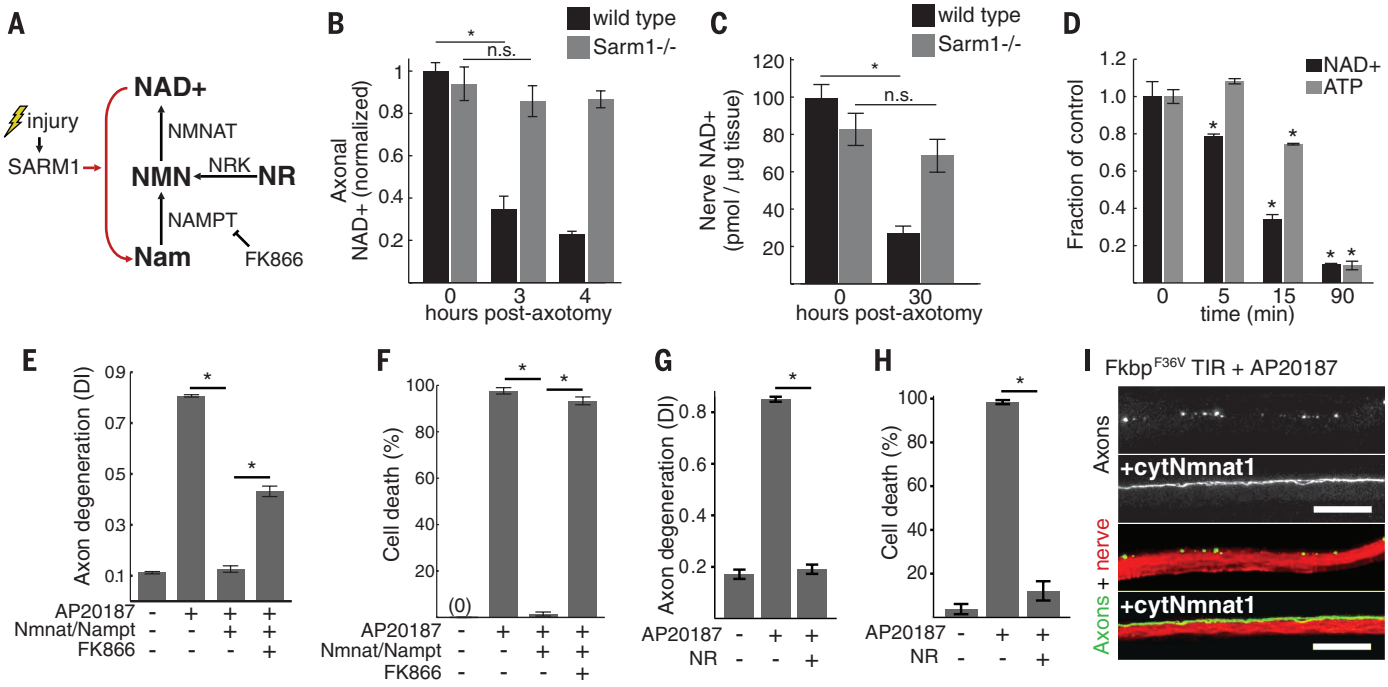

Fig. 3. Loss of NAD^+ underlies SARM1-induced destruction. (**A**) Diagram of NAD^+ synthesis and inhibition by FK866; Nrk, nicotinamide riboside kinase; NMN, nicotinamide mononucleotide. (**B**) Axonal NAD^+ concentration in cultured wild-type and $Sarm1^{-/-}$ DRG neurons after axotomy; normalized to wild-type control. (**C**) NAD^+ concentration in distal sciatic nerve segments from wild-type or $Sarm1^{-/-}$ animals after transection; wild-type $n = 5$; $Sarm1^{-/-}$ $n = 9$. (**D**) Neuronal NAD^+ and ATP concentrations after sTIR dimerization by AP20187; comparisons are made to 0 min control. (**E** and **F**) Axon degeneration (E) and neuronal cell death (F) induced by sTIR homodimerization (AP20187) and inhibition by NAD^+ synthetic enzymes with or without the Nampt inhibitor FK866 (10 nM); measured 24 hours after sTIR dimerization and FK866 application. (**G** and **H**) Effect of NR (1 mM) on axon degeneration (G) and neuronal cell death (H) induced by sTIR homodimerization (AP20187) for 24 hours with or without NR. (**I**) Micrographs showing sTIR-induced motor axon fragmentation in third-instar *Drosophila* larvae blocked by cytosolic Nmnat1 (cytNmnat1) expression. *M12-Gal4* drives expression from UAS-mCD8-GFP (green) and UAS-Fk^{F36V}TIR with or without UAS-cytNmnat1 in single motor axons in each nerve (red, HRP). Degeneration score = 76 ± 4% (control) versus 11 ± 2% (cytNmnat1); $P < 0.001$ (*t* test); scale bar, 20 µm. Error bars, SEM; $*P < 0.01$; one-way ANOVA with Tukey's post-hoc test.

To evaluate whether NAD^+ depletion alone is sufficient to induce axon destruction, we stimulated direct intracellular breakdown of NAD^+ by dimerization of the poly-ADP-ribose polymerase (PARP) domain of Tankyrase 1 (Tnkp; diagrammed in Fig. 4A). We generated dimerizable $Fkbp^{F36V}$-Tnkp and showed that AP20187 treatment of cells expressing this construct led to loss of NAD^+ and formation of PAR (fig. S7, A and B). In the presence of FK866, which inhibits de novo NAD^+ synthesis, Tnkp dimerization in dividing cells led to rapid energetic failure (ATP loss) that was blocked by the Tankyrase inhibitor XAV939 (fig. S7C). NR supplementation blocked toxicity but not PAR formation, indicating that NAD^+ loss and not PAR formation caused cell death (fig. S7, A and C). In neurons, Tnkp-induced depletion of NAD^+ caused degeneration of uninjured wild-type and $Sarm1^{-/-}$ axons (Fig. 4, B and C). Moreover, NAD^+ depletion from isolated (presevered) $Sarm1^{-/-}$ axons led to degeneration (Fig. 4C). Thus, rapid NAD^+ depletion is sufficient to cause rapid axon loss.

To define whether SARM1-mediated depletion of NAD^+ results from increased consumption or decreased synthesis of NAD^+, we introduced exogenous NAD^+ and, as a control, nicotinic acid adenine dinucleotide (NaAD) into HTir cells by electroporation (*15*), followed by sTIR dimerization. Control cells showed rapid loss of endogenous NAD^+ within 5 min in response to sTIR dimerization. Electroporation in the presence of NAD^+ increased the concentration of NAD^+ by a factor of 4.3, but NAD^+ was rapidly consumed upon sTIR dimerization. The specificity of this reaction is highlighted by the stability of the closely related analog NaAD (Fig. 4D). sTIR-induced loss of NAD^+ thus involves the active consumption of NAD^+. We next demonstrated that the consumed NAD^+ is converted to nicotinamide (Nam). When radiolabeled ^{14}C-NAD^+ was introduced into cells, 15 min of sTIR dimerization elicited loss of ^{14}C-NAD^+ and concomitant increases in ^{14}C Nam as detected by thin-layer chromatography (Fig. 4E). Similarly, sTIR dimerization in nonelectroporated cells also elicited Nam release as detected by HPLC (fig. S8).

Rapid breakdown of NAD^+ induced by SARM1 TIR is similar to that observed when PARP is activated in response to DNA damage (*16*). However, NAD^+ breakdown induced by sTIR is PARP-independent. The PARP inhibitor olaparib reduced NAD^+ loss induced by H_2O_2, but had no effect on SARM1-induced loss of NAD^+ (Fig. 4F). Furthermore, H_2O_2 led to PARP-dependent accumulation of PAR, whereas no PAR was detected after sTIR dimerization (Fig. 4F). Finally, sTIR dimerization in $Parp1^{-/-}$ cells induced loss of NAD^+, axon degeneration, and cell death (fig. S9). These cell-destruction phenotypes were also unaffected by genetic ablation of the NAD^+ glycohydrolase CD38, another major consumer of NAD^+ (*17*) (fig. S9). SARM1 therefore initiates an NAD^+ breakdown program that drives axon destruction and cell death independently of PARP1 and CD38.

SARM1 and its orthologs promote axonal degeneration (*5*, *6*) as well as neuronal (*18*–*20*) and non-neuronal (*21*, *22*) cell death. SARM1-induced breakdown of NAD^+ links axon degeneration to the axon-protective Wld^S protein. The presence of Wld^S or other sources of axonal Nmnat may allow for rapid resynthesis of NAD^+ and the maintenance of metabolic function, thereby counteracting the destructive effects of NAD^+ degradation by SARM1. Identification of a class of neuroprotective drugs that increase NAD^+ biosynthesis through effects on Nampt have highlighted the therapeutic potential of augmented NAD^+ synthesis in neurological disorders (*23*). Our study provides further biological rationale for NAD^+ augmentation as a therapeutic approach. Inhibition of SARM1-mediated NAD^+ loss may be an alternative or synergistic therapeutic strategy for the treatment of neurologic disorders.

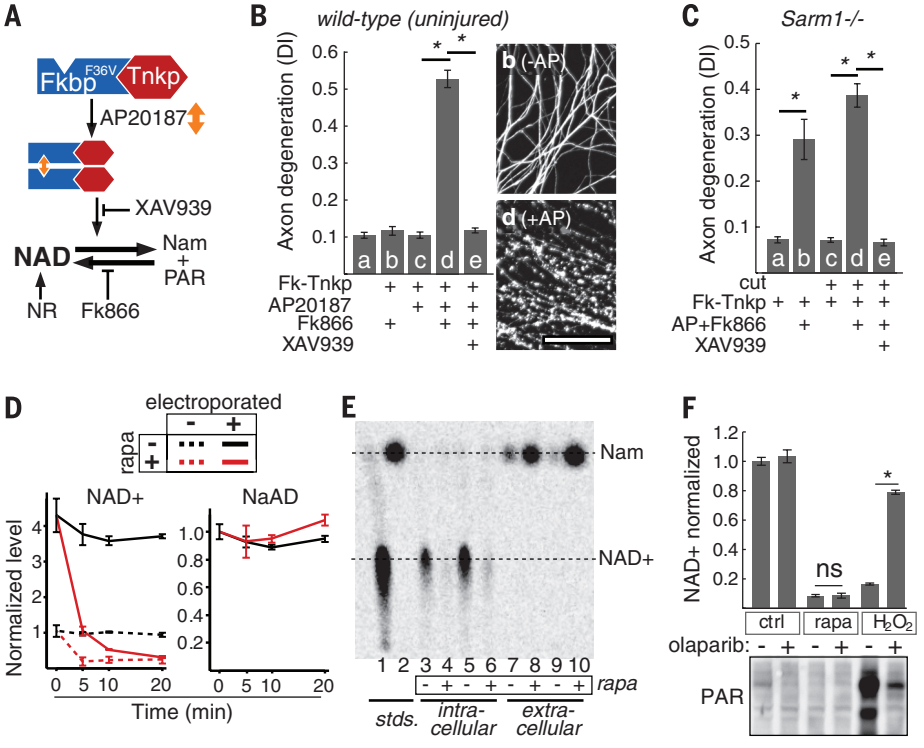

Fig. 4. Effects of NAD^+ breakdown on axon degeneration. (**A**) Diagram of NAD^+ manipulation using Tnkp dimerization. NAD^+ loss induced by FkbpF36V-Tnkp dimerization is blocked by Tankyrase inhibitor XAV939 or NR and is exacerbated by FK866. (**B**) Axon degeneration in response to NAD^+ depletion by dimerized Tnkp and FK866 after 24 hours (bar d) and inhibition by Tankyrase inhibitor XAV939 (100 nM; bar e). Representative α-tubulin–stained axons corresponding to bars b and d are shown; scale bar, 50 μm. (**C**) Effect of NAD^+ depletion by dimerized Tnkp + FK866 on axon degeneration in $Sarm1^{-/-}$ uninjured axons (bar b) or isolated (cut) $Sarm1^{-/-}$ axons (bar d). (**D**) Effect of sTIR dimerization on endogenous (dotted lines) and exogenously introduced (solid lines) NAD^+ or NaAD (control) in HTir cells. NaAD is undetectable in nonelectroporated cells. (**E**) Conversion of ^{14}C-NAD^+ in HTir cells to Nam 15 min after SARM1 TIR dimerization. NAD^+ and Nam from cell extracts and extracellular media were resolved by thin-layer chromatography. (**F**) (Top) Effect of the PARP inhibitor olaparib (100 nM) on NAD^+ loss induced by 1 mM H_2O_2 (10 min) or sTIR dimerization (10 min) in HTir cells. (Bottom) PAR formation after H_2O_2 treatment or sTIR dimerization in HTir cells expressing PARG shRNA and inhibition by olaparib. Error bars, SEM; *$P < 0.01$; one way ANOVA with Tukey's post-hoc test.

REFERENCES AND NOTES

1. Y. Fuchs, H. Steller, *Cell* **147**, 742–758 (2011).
2. L. Conforti, J. Gilley, M. P. Coleman, *Nat. Rev. Neurosci.* **15**, 394–409 (2014).
3. M. P. Coleman *et al.*, *Proc. Natl. Acad. Sci. U.S.A.* **95**, 9985–9990 (1998).
4. T. Araki, Y. Sasaki, J. Milbrandt, *Science* **305**, 1010–1013 (2004).
5. J. M. Osterloh *et al.*, *Science* **337**, 481–484 (2012).
6. J. Gerdts, D. W. Summers, Y. Sasaki, A. DiAntonio, J. Milbrandt, *J. Neurosci.* **33**, 13569–13580 (2013).
7. L. A. O'Neill, K. A. Fitzgerald, A. G. Bowie, *Trends Immunol.* **24**, 286–289 (2003).
8. M. C. Wehr *et al.*, *Nat. Methods* **3**, 985–993 (2006).
9. J. Y. Kang, J.-O. Lee, *Annu. Rev. Biochem.* **80**, 917–941 (2011).
10. A. Fegan, B. White, J. C. T. Carlson, C. R. Wagner, *Chem. Rev.* **110**, 3315–3336 (2010).
11. Y. Sasaki, J. Milbrandt, *J. Biol. Chem.* **285**, 41211–41215 (2010).
12. J. Wang *et al.*, *J. Cell Biol.* **170**, 349–355 (2005).
13. Y. Sasaki, B. P. S. Vohra, F. E. Lund, J. Milbrandt, *J. Neurosci.* **29**, 5525–5535 (2009).
14. A. Nikiforov, C. Dölle, M. Niere, M. Ziegler, *J. Biol. Chem.* **286**, 21767–21778 (2011).
15. M. C. Elia, L. E. Motyka, T. D. Stamato, *Anal. Biochem.* **192**, 329–333 (1991).
16. M. Y. Kim, T. Zhang, W. L. Kraus, *Genes Dev.* **19**, 1951–1967 (2005).
17. P. Aksoy, T. A. White, M. Thompson, E. N. Chini, *Biochem. Biophys. Res. Commun.* **345**, 1386–1392 (2006).
18. Y. Kim *et al.*, *J. Exp. Med.* **204**, 2063–2074 (2007).

19. P. Mukherjee, T. A. Woods, R. A. Moore, K. E. Peterson, *Immunity* **38**, 705–716 (2013).
20. D. W. Summers, A. DiAntonio, J. Milbrandt, *J. Neurosci.* **34**, 9338–9350 (2014).
21. E. S. Blum, M. C. Abraham, S. Yoshimura, Y. Lu, S. Shaham, *Science* **335**, 970–973 (2012).
22. P. Panneerselvam *et al.*, *Cell Death Differ.* **20**, 478–489 (2013).
23. G. Wang *et al.*, *Cell* **158**, 1324–1334 (2014).

ACKNOWLEDGMENTS

Supported by National Institutes of Health grants RO1DA020812 (A.D.), RO1AG013730 (J.M.), RO1NS065053, RO1NS087632, and RO1NS078007 (J.M. and A.D.), and F31NS074517 (J.G.); and a grant from Vertex Pharmaceuticals. We thank ChromaDex (Irvine, California) for providing nicotinamide riboside; A. Strickland, T. Farhner, and N. Panchenko for technical assistance; and members of the Milbrandt and DiAntonio labs for fruitful discussions.

SUPPLEMENTARY MATERIALS

www.sciencemag.org/content/348/6233/453/suppl/DC1
Materials and Methods
Supplementary Text
Figs. S1 to S9
References (*24*–*27*)

7 July 2014; accepted 12 March 2015
10.1126/science.1258366

RIBOSOME

Mechanical force releases nascent chain–mediated ribosome arrest in vitro and in vivo

Daniel H. Goldman,[1]* Christian M. Kaiser,[2,3]*† Anthony Milin,[1,3] Maurizio Righini,[2] Ignacio Tinoco Jr.,[1] Carlos Bustamante[1,2,4,5,6,7]†

Protein synthesis rates can affect gene expression and the folding and activity of the translation product. Interactions between the nascent polypeptide and the ribosome exit tunnel represent one mode of regulating synthesis rates. The SecM protein arrests its own translation, and release of arrest at the translocon has been proposed to occur by mechanical force. Using optical tweezers, we demonstrate that arrest of SecM-stalled ribosomes can indeed be rescued by force alone and that the force needed to release stalling can be generated in vivo by a nascent chain folding near the ribosome tunnel exit. We formulate a kinetic model describing how a protein can regulate its own synthesis by the force generated during folding, tuning ribosome activity to structure acquisition by a nascent polypeptide.

The ribosome translates mRNA into amino acid sequences that contain the information needed for the polypeptide to attain its native structure. Differential usage of synonymous codons and structural elements in the mRNA modulate polypeptide elongation rates. Such rate variations may be required for proper folding and processing of nascent proteins (*1*). Moreover, interactions of specific nascent chain sequences (*2*, *3*) with the ribosome exit tunnel (*4*) result in reduced rates of elongation. The bacterial SecM protein represents an example of a stalling sequence that interacts with the ribosome exit tunnel and allosterically represses the peptidyl transferase activity of the ribosome (*4*–*7*). Translation of SecM regulates expression of SecA, the motor component of the bacterial Sec translocon (*2*). Release of stalling in vivo requires interactions between nascent SecM and the translocon machinery (*8*, *9*). It has been suggested that mechanical force exerted by the translocon relieves elongation arrest and leads to translation restart (*10*).

To investigate the effect of force on the release of SecM-stalled ribosome–nascent chains (RNCs), we adapted a single-molecule optical tweezers assay (*11*) (Fig. 1A), enabling the application of defined forces to single ribosome-associated nascent polypeptides. We generated stalled RNCs that contained the C-terminal domain of human calmodulin (CaM) (figs. S1 and S2). CaM provides a mechanical fingerprint (*12*) in our experiments by exhibiting equilibrium folding and unfolding ("hopping") at ~7 pN (Fig. 1B and supplementary materials). To detect release of stalled ribosomes, we used the antibiotic puromycin. Puromycin binds to the ribosomal A site and is incorporated into the nascent polypeptide, leading to its release from the ribosome (*13*). SecM-arrested ribosomes, containing a prolyl-tRNA^{Pro} stably bound in the A site, are refractory to treatment with puromycin, but become sensitive after arrest release, proline incorporation, and translocation (*14*) (figs. S3 and S4). In the presence of puromycin and EF-G, arrest release will become apparent as a rupture of the tether (Fig. 1B and fig. S4).

We applied a defined, constant force to the molecule in the range of 10 to 30 pN and measured the time required to restart translation, as measured by tether rupture. The mean restart times decreased with increasing force (Fig. 1C). We calculated the rate of stalling rescue as a function of the applied force (Fig. 1, C and D, and figs. S5 and S6). By fitting the force-dependent rates to Bell's model (*15*), we estimated a distance to the transition state ($\Delta x^{\ddagger}$) of 0.4 nm [95% confidence interval (CI): 0.1 nm, 0.8 nm] and a zero-force rupture rate (k_0) of 3×10^{-4} s^{-1} (95% CI: 0.5×10^{-4} s^{-1}, 20×10^{-4} s^{-1}). This rate is in agreement with biochemical ensemble experiments, in which no force was applied (Fig. 1D, blue dot and fig. S3). In the force range of our experiments, release of SecM-mediated arrest is accelerated by more than an order of magnitude (Fig. 1D), supporting the hypothesis that SecM arrest is relieved by the mechanical force generated by the SecA adenosine triphosphatase (ATPase).

Cotranslational insertion of transmembrane helices via the translocon can release SecM-mediated stalling, presumably by generating force (*16*). We wondered whether folding of a nascent globular protein domain could generate a force capable of modulating elongation by acting on peptide-tunnel interactions. Such interactions could serve to tune elongation rates to folding transitions (*3*, *4*). The exit tunnel is too narrow to accommodate folded protein domains (*17*); therefore, as a nascent polypeptide emerges from the exit tunnel and folds in close proximity to the ribosome, it will be sterically excluded from the tunnel. This steric exclusion might generate a force that pulls on the nascent chain within the exit tunnel, which could modulate ribosome activity.

Having established that force accelerates SecM arrest release, we used SecM as a sensor to detect if nascent protein folding outside the ribosome can release the arrest. We constructed a library of plasmids encoding fusion proteins in which the stalling sequence (SecM17) is separated from the de novo–designed protein Top7 (*18*) by flexible linker sequences of various lengths, followed by a reporter green fluorescent protein (GFP) (Fig. 2A, fig. S7, and supplementary materials). Top 7 folds rapidly against an applied force in close proximity to the ribosome (fig. S8). The GFP coding sequence is translated only upon successful release of the SecM17-mediated translation arrest. Variations in the length of the linker separating Top7 and SecM17 would affect the translation outcome of these constructs (Fig. 2B). Short linker sequences will not allow folding of Top7 because the C terminus of the protein will be sequestered in the exit tunnel (Fig. 2B, top). Intermediate-length linkers will allow more of the Top7 sequence to emerge from the ribosome tunnel and for the protein to fold and produce the steric exclusion folding force (Fig. 2B, middle). And while longer

[1]Department of Chemistry, University of California, Berkeley, CA 94720, USA. [2]Institute for Quantitative Biosciences (QB3), University of California, Berkeley, CA 94720, USA. [3]Department of Biology, Johns Hopkins University, Baltimore, MD 21218, USA. [4]Department of Physics, University of California, Berkeley, CA 94720, USA. [5]Department of Molecular and Cell Biology, University of California, Berkeley, CA 94720, USA. [6]Kavli Energy Nanosciences Institute at Berkeley, Berkeley, CA 94720, USA. [7]Howard Hughes Medical Institute, University of California, Berkeley, CA 94720, USA.
*These authors contributed equally to this work. **†Corresponding author. E-mail: carlos@alice.berkeley.edu (C.B.), kaiser@jhu.edu (C.M.K.)**

SARM1 activation triggers axon degeneration locally via NAD$^+$ destruction

Josiah Gerdts, E.J. Brace, Yo Sasaki, Aaron DiAntonio and Jeffrey Milbrandt

Science **348** (6233), 453-457.
DOI: 10.1126/science.1258366

SARM1-driven axon degeneration

Axons, the long protrusions of nerve cells, are programmed to self-destruct under certain conditions that occur during development, stress, or disease states. Gerdts *et al.* outline a biochemical mechanism that controls such axon degeneration. The authors designed versions of SARM1 (sterile alpha and TIR motif—constraining 1) that could be activated or inhibited in cells. Their experiments showed that the activation of SARM1 was necessary and sufficient to cause axon destruction in cultured mouse neurons. SARM1-mediated destruction was associated with depletion of the metabolic cofactor NAD $^+$ from cells.

Science, this issue p. 453